ELSEVIER

Thermochimica Acta 391 (2002) 137–150

thermochimica acta

www.elsevier.com/locate/tca

Trehalose dehydration under confined conditions

Fabiana Sussich, Saní Bortoluzzi, Attilio Cesàro*

Department of Biochemistry, Biophysics and Macromolecular Chemistry, Laboratory of Physical and Macromolecular Chemistry and INSTM, UdR Trieste, University of Trieste, Via Giorgeri 1, I-34127 Trieste, Italy

Received 5 October 2001; received in revised form 30 January 2002; accepted 20 February 2002

Abstract

A DSC study of the dehydration process of trehalose dihydrate (TRE_h) crystals has been carried out by tuning scanning rates of the product formation, under "controlled evaporation rates" (confined conditions). The rationale for this study is the construction of a dynamic diagram as a function of the time scale of trehalose transformations and the timescale of water effusion.

Results at different rates of heating and of water evaporation indicate that only dehydration of TRE_h crystals and melting of the TRE_β form are constantly present. Amorphous state can be thermally produced under different ways: (a) by direct amorphisation of TRE_h; (b) by passing through the TRE_α form; (c) by cooling the liquid formed after TRE_β melting. The anhydrous TRE_α form is produced from TRE_h under gentle conditions of low scanning rates (large transformation times) and high evaporation rates (low humidity) even at relatively low temperatures (60 °C).

Keywords: Dehydration; DSC; Dynamic transformation diagram; Trehalose

1. Introduction

Polymorphism of crystalline sugars and dehydration of their hydrate forms are an intriguing matter that is receiving much attention for many practical implications. It is also a fuzzy scientific problem which needs careful and detailed study for the assessment of the interconversion paths and the relative stabilities of the several polymorphic forms [1–3].

Among carbohydrate molecules, trehalose has been studied in different laboratories, mainly for its fundamental physical role as bioprotector (for a review see [4]). Glass transition and aqueous solution properties of trehalose are considered mostly relevant to the bioprotective action against biopolymer denaturation [5] and cellular shrinking of plant tissues [6]. Biosynthesis, biological activity and metabolic pathway of trehalose [7] in micro-organisms naturally producing this molecule, are of great interest for the exploitation of exogenous bioprotective activity.

The first attempt to characterise thermodynamic properties of trehalose crystalline polymorphs [8] has immediately brought attention to the subtle dependence of the polymorphic interconversions with the heating rates and to the interplay of water removal on the structural rearrangements [9,10]. It was reported that trehalose properties, produced after a dehydration process, strongly depend on the experimental conditions. The concept of "time window for water plasticisation while escaping from the crystalline structure" has been used to underline the delicate dynamic balance between structural shaking and water hopping [8]. Production of amorphous form can be a consequence of drying,

* Corresponding author. Tel.: +39-040-5583684; fax: +39-040-5583691.
E-mail address: cesaro@univ.trieste.it (A. Cesàro).

0040-6031/02/$ – see front matter
PII: S0040-6031(02)00171-5

cooling, milling and other energetic routes [8,11,12] and is an important matter for pharmaceutical products [13]. Personal communications from other laboratories (H. Suga, Osaka, Japan and M. Descamps, Lille, France) were also in agreement with the relevance of scanning rates for ensuring a controlled transformation. Other literature reports dealt with several spectroscopic properties (mainly IR, Raman and NMR) [14–16] of trehalose polymorphic forms, although the preparation of the samples is not always consistent.

Attempts to classify the solid state dehydration refer mainly to inorganic salts and criteria for classification have been recently reviewed by Galwey [17]. However, the complexity of the transformations occurring during and/or after trehalose dehydration appears still at a phenomenological stage.

Transitions between the different trehalose polymorphs have been assessed and the relative values of ΔH and temperatures have been reported [10]. However, in a previous work [9], it was underlined the importance of clarifying the changes of pathway and the extent of transformations induced by external variables. Nowadays, the world-wide aim of the trehalose research is to understand the mechanism involved in the trehalose ability to protect cells with its structural transformations. In this paper, a DSC study of the dehydration phenomenon has been carried out by controlling the most relevant variables. The aim was to investigate the dependence on the scanning rates of the product formation under ''controlled evaporation rates'' (confined conditions).

2. Experimental

2.1. Materials

Trehalose dihydrate (TRE_h) was obtained from Sigma Chemical Co. and was used without further purification. Two anhydrous forms, TRE_α and TRE_β, were prepared as previously described [8,9], keeping the dihydrate sample under vacuum at 85 and at 130 °C for 4 h, respectively. A third crystalline form, TRE_γ, [9] was produced directly in the calorimeter by heating the TRE_h up to the water loss and by stopping the scan at the subsequent cold crystallisation, at a temperature around 115 °C; the specimen was then quenched to room temperature.

2.2. Calorimetric measurements

Calorimetric measurements were carried out with a Perkin-Elmer DSC 6. The Pyris software version 3.81 from Perkin-Elmer was used with the Windows NT 3.5. The thermal unit was thermostated with an external thermocryostat in which the coolant was kept at 0 °C; a nitrogen flux (20 ml/min) was used as a purge gas for the furnace. Temperature and heat flow calibrations were carried out according to standard procedures for DSC6.

3. Results and discussion

3.1. Preliminary characterisation of the polymorphs

Depending on the thermal treatment, TRE_h undergoes different polymorphic transformations giving origin to either partially hydrated or anhydrous crystalline and amorphous forms. The schematic picture of the transformation paths is illustrated in Fig. 1A (adapted from [4]). TRE_α is linked to the parent TRE_h by a topotactic relationship [4,8]. TRE_γ is prepared only during a DSC heating scan (20 K/min) and by stopping the heating at about 115 °C, during the exothermic crystallisation.

Although description of the thermal behaviour of trehalose polymorphs has already been given in the literature, it is here briefly reviewed only for safety of clarification for their identification. Each of the four different forms present characteristic measured curves, which have been analysed in details at different scan rates [10]. Fig. 1B shows the shape of the curves that have constantly been reproduced in our laboratory for the trehalose polymorphs with several DSC apparatuses (both power compensation and heat flow types). Transition temperatures, transition enthalpies and non-equilibrium cold crystallisation phenomena have well-defined values (Table 1) and contribute to the fingerprinting of trehalose polymorphs.

Since this work deals with the transformations of TRE_h form, some previous experiments have been rerun in order to show consistency of the results of the new trehalose batch with original data. This concern is necessary in view of some discrepancies mentioned in the literature and possibly attributed to different size and/or preparation of the crystals [18,19].

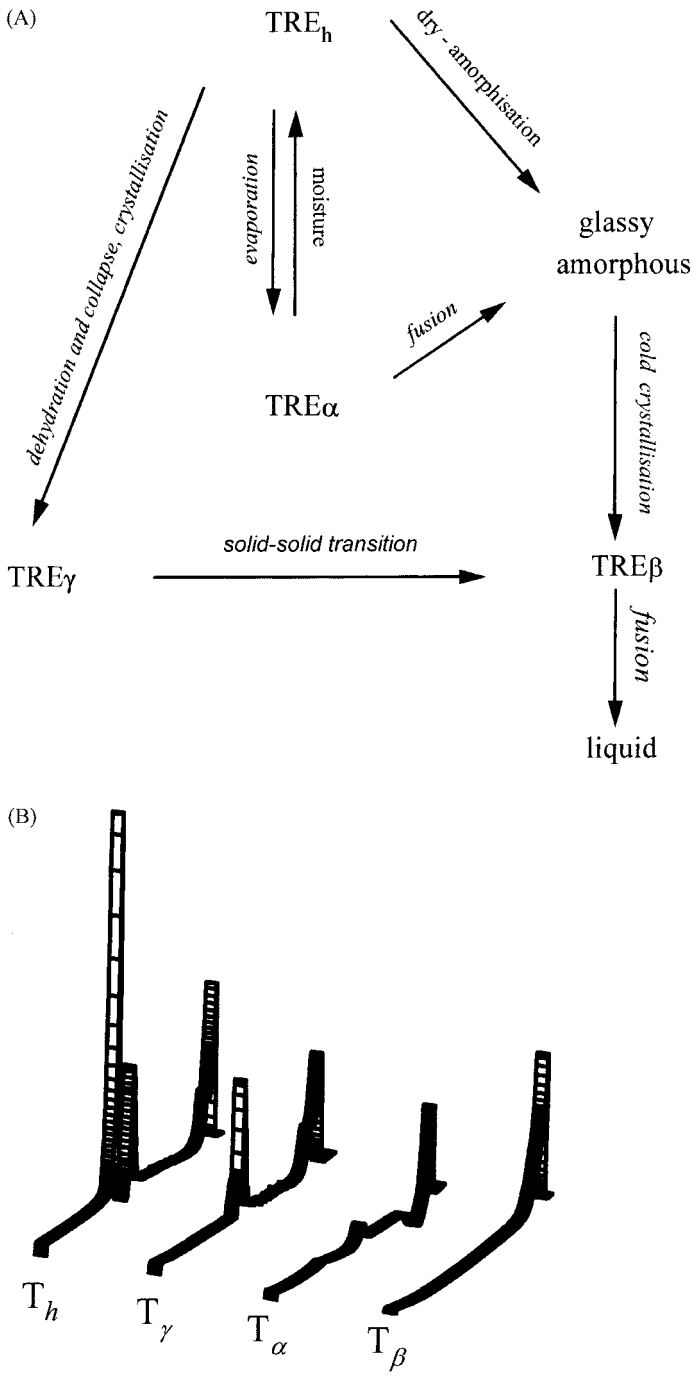

Fig. 1. Schematic representation of trehalose interconversions (adapted from [4]). (A) The transition TRE_h–TRE_α is reversible; TRE_α is linked to the parent TRE_h by a topotactic relationship [4,8]; (B) DSC curves of trehalose polymorphs heated at 20 K/min. Dehydration of TRE_h occurs via the formation of TRE_γ.

Table 1
Thermodynamic data for transitions of trehalose polymorphs

Transition	T[a] (K, °C)	ΔH (kJ/mol)
$TRE_h \rightarrow$ amorphous (dehydration)	373.1 (100) ± 0.5	113.5
$TRE_\gamma \rightarrow TRE_\beta$ (transition)	385.0 (111.9) ± 1	33.1 ± 2.5
$TRE_\alpha \rightarrow TRE_{am}$ (melting)	394.6 (121.5) ± 1.3	5.8
$TRE_{am} \rightarrow TRE_\beta$ (crystallisation)	453.5 (180.4) ± 3	−44.9
$TRE_\beta \rightarrow TRE_L$ (melting)	479.9 (206.8) ± 0.1	51.3 ± 2

Errors are not reported for transition enthalpies involving the amorphous TRE_{am} state.
[a] Onset temperature.

3.2. Standardisation of orifice rate of effusion

In addition to checking for the reproducibility of the experimental procedures and of polymorph preparations, calorimetric experiments have been carried out to "qualitatively calibrate" the time/temperature domain for the process of water evaporation and flowing through the cell orifices of different sizes. Orifices in the cell caps have been duly measured to range from 0.1 to 1.2 mm; additional experiments were done with sealed cells and with uncovered (open) cells.

Evaporation of water has been used to simulate the flowing-through process (effusion). These data are presented here in order to provide a reference scale for the effect of different experimental conditions (orifice sizes) on trehalose dehydration and not for a quantitative discussion about the dynamics of water evaporation and effusion.

Fig. 2 shows the linear dependence of the heat flow measured at 35 °C on the square orifice radius. Given the dependence of the overall flowing kinetic upon the size of the orifice, the heat flow at any given temperature is related to vapour pressure and to the square of the radius orifice. This means that the residence time of vapour is related to the orifice size and that, under suitable condition, is also function of temperature.

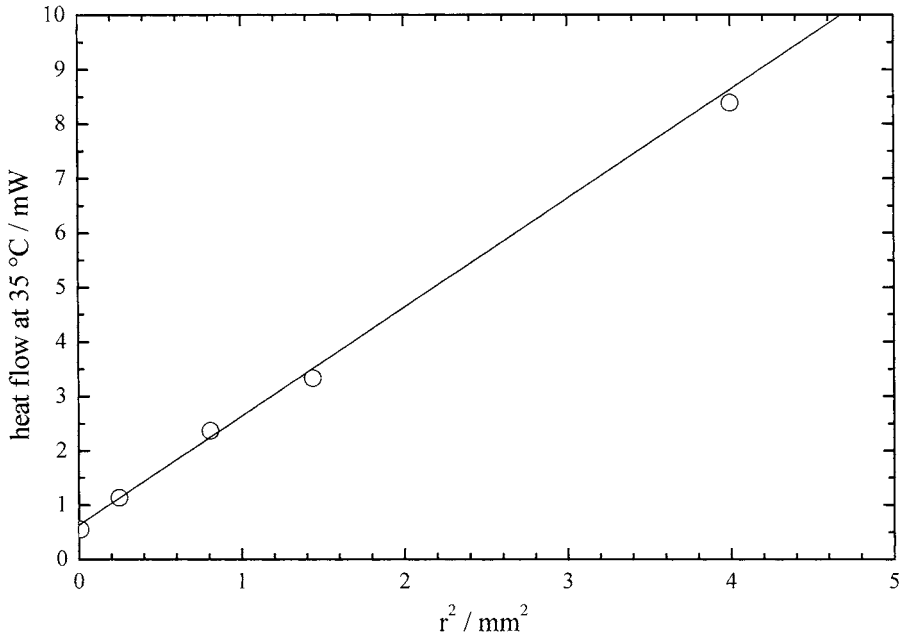

Fig. 2. DSC of water evaporation by using cells with different orifice radius (0.1, 0.5, 0.9, 1.2 and 2 mm) showing the dependence of the heat flow (at 35 °C) on the square of orifice radius.

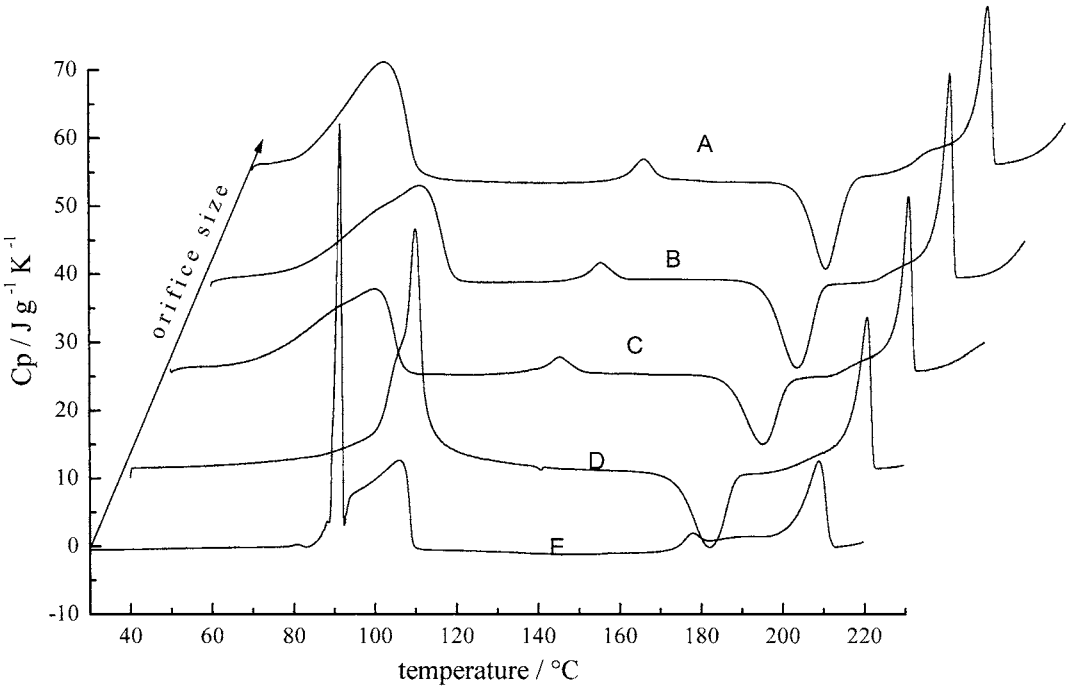

Fig. 3. Set of TRE_h heated at 1 K/min by using cells with different orifice radius. Curve A refers to open cell; curves B–E have orifice size of 1.2, 0.9, 0.5 and 0.1 mm, respectively. Residence time of water vapour inside the cell tunes the type of structure being formed.

Therefore, the orifice size seems to be an operative parameter in controlling the process of dehydration/evaporation.

3.3. Trehalose dehydration as a function of orifice rate of effusion

Before analysing the effect of the scanning rate, thermograms at constant scanning rate of 1 K/min are reported (Fig. 3) for each orifice radius. Since in all respects a small orifice is a ''constrain'' to free evaporation, the concept of ''confined dehydration'' has therefore to be introduced, in order to focus the readers' attention on the actual meaning behind these experimental set-ups.

Fig. 3 shows a set of thermograms recorded with different orifices. Measurements have been done in the range between 30 and 230 °C, and each experiment was repeated many times (from 4 to 7 times), in order to check for reproducibility. Assignment of the thermal events is made on the basis of previous findings, which are corroborated by the SWAXS results recorded on-line by using the ELETTRA synchrotron radiation facility during the heating scans (paper in preparation).

Curves marked A, B and C (open cell, 1.2 and 0.9 mm orifice, respectively) show a similar behaviour: a broad endotherm below 100 °C indicates the dehydration process, followed by a small bump in the region 120–130 °C, which is tentatively associated with the melting of TRE_α, produced after dehydration. Above 150 °C, the amorphous phase becomes unstable and undergoes cold crystallisation between 160 and 180 °C. Eventually, the stable crystalline TRE_β melts at temperatures above 200 °C.

Upon decreasing orifice size, changes in the thermogram shape are evident. With orifice D (0.5 mm), amorphisation is obtained upon dehydration, being the transition of TRE_α absent. The cold crystallisation and final melting events are similar to those reported for samples A, B and C.

Further decreasing of the orifice size to 0.1 mm (curve E), makes the dehydration peak highly asymmetric, with a sharp spike at low temperature followed by a small exothermic signal before completion of dehydration is observed. No evidence of a clear cold

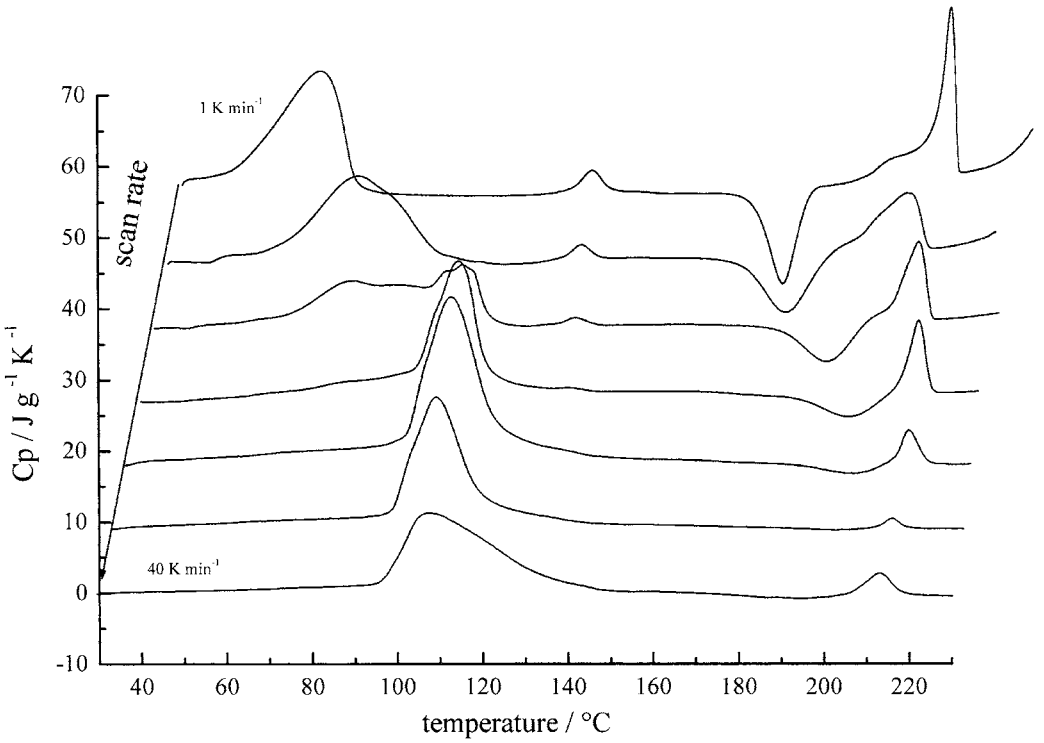

Fig. 4. DSC curves of TRE_h heated in open pans. Different curves refer to different scan rates (at 1, 2, 5, 10, 20, 30 and 40 K/min). Low scan rates (long transformation times) lead to TRE_α, while high scan rates induce amorphisation.

crystallisation is present, although the final melting peak of TRE_β is still shown. A continuous slow reorganisation of the amorphous phase probably occurs, being small nuclei formed before complete dehydration.

3.4. Trehalose dehydration as a function of scanning rate and orifice size

Having assessed the difference of thermal behaviour on the basis of the orifice size, the effect of changing scanning rate for the different orifices has been studied, including open pans and hermetically sealed pans.

When heated in open pans at high scan rates, TRE_h shows only the dehydration peak slightly above 100 °C and a small endothermic effect in the temperature range of melting of TRE_β (Fig. 4). Upon decreasing scanning rate, longer transformation time allows the formation of TRE_α after the dehydration, then TRE_α melts into an amorphous phase which undergoes crystallisation to TRE_β. The final melting of TRE_β occurs above 200 °C. The slower scanning facilitates these phenomena, the small bump of TRE_α melting appearing at scan rates smaller than 10 K/min. The DSC data are collected in Table 2.

Cells with orifice size of 1.2 mm give the same results as those with 0.9 mm (Table 3), the only difference being the minor entity of the phenomenon between 100 and 120 °C by using the orifice of 1.2 mm. Fig. 5 displays the thermograms obtained by using the 1.2 mm orifice: for 1 and 2 K/min the first endothermic peak is due to both dehydration and conversion toward the crystalline form TRE_α. By increasing the scan rate, the thermal behaviour becomes different and more complex: after dehydration there is the characteristic concomitant transition of melting–crystallisation–melting, which is more evident in the thermograms.

Samples placed in cells with caps with a hole of 0.5 mm show (Fig. 6 and Table 4) a behaviour that for all the scan rates, except for 1 K/min, is similar to those of Fig. 5 (at high scan rates). At low scan rate

Table 2

Scan rate (K/min)	T_p (°C)	ΔH (kJ/mol)	T_p (°C)	ΔH (kJ/mol)	T_p (°C)	ΔH (kJ/mol)	T_p (°C)	ΔH (kJ/mol)
	$TRE_h \rightarrow TRE_\alpha$		$TRE_\alpha \rightarrow TRE_{am}$		$TRE_{am} \rightarrow TRE_\beta$		$TRE_\beta \rightarrow TRE_L$	
1	65.7	106.7	126.1	8.4	170.7	−41.5	210.8	50.6
2	74.8	109.8	127.0	5.9	176.0	−41.5	206.7	38.7
5	103.4	110.3	128.7	2.3	187.5	−32.5	209.3	25.4
	$TRE_h \rightarrow TRE_{am}$				$TRE_{am} \rightarrow TRE_\beta$		$TRE_\beta \rightarrow TRE_L$	
10	104.5	116.5			196.1	−22.5	212.7	17.1
20	106.3	123.5			200.1	−7.9	213.5	7.1
30	106.9	114.5			199.7	−3.3	212.5	2.4
40	107.1	107.7			194.3	−5.3	212.7	6.0

Temperature and enthalpy changes for the transitions of trehalose at different scan rates.

(1 K/min) dehydration is associated with an amorphisation of the sample (see the cold crystallisation below 180 °C of the amorphous phase), while faster heatings lead to the phenomenon of melting–crystallisation–melting between 100 and 140 °C. The latter behaviour is linked to the formation of TRE_γ, which has been identified as a core of TRE_h with an outer layer of TRE_β [9], produced by a mechanism often called "orange peel structure" formation [17]. The production of TRE_γ is less evident increasing the scanning rate and disappears at 40 K/min. All thermograms, as usual, show the melting of TRE_β.

With the cells of the smallest orifice size (0.1 mm), all the thermograms (Fig. 7) show some common transitions, clearly highlighted by two endothermic peaks, in the temperature range 90–140 °C, and by a third one above 180 °C (Table 5). At low scan rate the two peaks are not resolved, the first one is very sharp

Table 3

Scan rate (K/min)	T_p (°C)	ΔH (kJ/mol)	T_p (°C)	ΔH (kJ/mol)	T_p (°C)	ΔH (kJ/mol)	T_p (°C)	ΔH (kJ/mol)
	$TRE_h \rightarrow TRE_\alpha$		$TRE_\alpha \rightarrow TRE_{am}$		$TRE_{am} \rightarrow TRE_\beta$		$TRE_\beta \rightarrow TRE_L$	
1	79.1	121.1	125.5	6.8	173.9	−40.9	211.2	47.0
2	104.0	108.8	128.5	1.2	176.6	−41.3	205.3	29.6
	$TRE_\beta \rightarrow TRE_L$				$TRE_{am} \rightarrow TRE_\beta$		$TRE_\beta \rightarrow TRE_L$	
5	103.7	127.4			186.6	−36.1	209.7	27.5
	$TRE_h \rightarrow TRE_{anh}$		$TRE_{anh} \rightarrow TRE_\gamma$		$TRE_\gamma \rightarrow TRE_\beta$		$TRE_h \rightarrow TRE_{am}$	
10	104.8	75.1	111.4	−2.6	118.5	15.0	209.7	45.3
20	107.5	71.4	118.2	−2.4	125.0	15.1	212.4	45.1
30	106.5	72.2	120.7	−1.5	127.5	17.1	213.2	44.7
40	108.2	66.8	123.1	−0.1	130.7	18.6	214.4	42.1
	$TRE_h \rightarrow TRE_\alpha$		$TRE_\alpha \rightarrow TRE_{am}$		$TRE_{am} \rightarrow TRE_\beta$		$TRE_\beta \rightarrow TRE_L$	
1	83.8	113.5	125.3	6.5	172.3	−42.5	209.8	47.8
2	104.0	116.1	128.3	1.0	176.6	−39.0	205.1	28.6
	$TRE_h \rightarrow TRE_{am}$				$TRE_{am} \rightarrow TRE_\beta$		$TRE_\beta \rightarrow TRE_L$	
5	102.5	116.5			188.1	−31.2	209.6	25.8
	$TRE_h \rightarrow TRE_{anh}$		$TRE_{anh} \rightarrow TRE_\gamma$		$TRE_\gamma \rightarrow TRE_\beta$		$TRE_\beta \rightarrow TRE_L$	
10	104.1	67.7	110.7	−5.3	122.3	18.9	210.0	44.3
20	105.7	62.7	114.9	−4.0	122.8	27.4	213.3	44.4
30	106.7	64.0	118.3	−2.5	125.7	27.8	214.0	44.7
40	108.0	59.7	121.7	−0.2	130.5	28.6	215.7	43.5

Temperature and enthalpy changes for the transitions of trehalose at different scan rates.

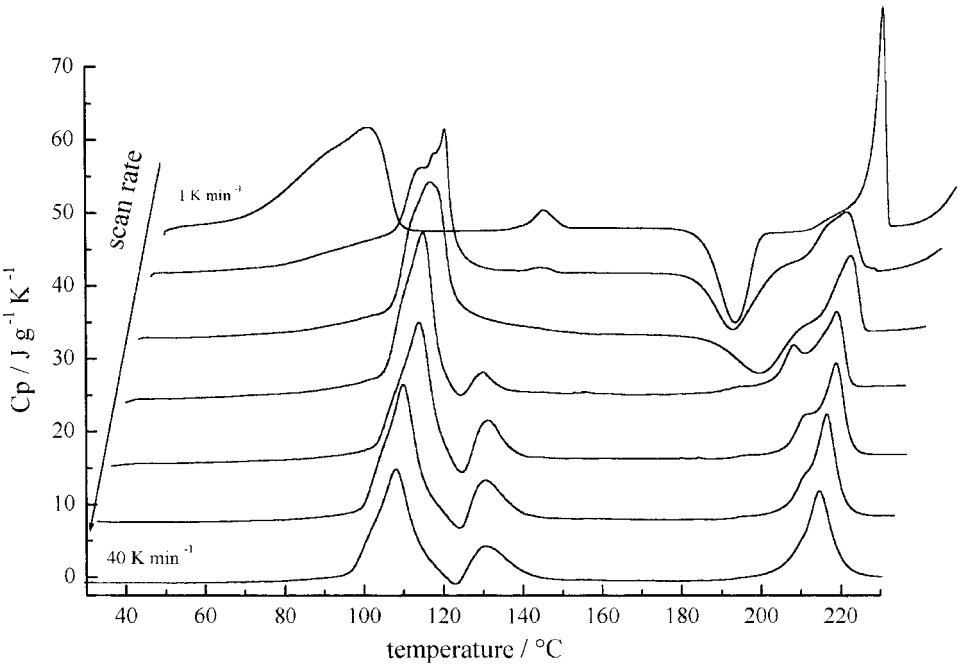

Fig. 5. DSC curves of TRE_h heated in cells with 1.2 mm orifice size at different scan rates (as in Fig. 4). Similar results are obtained with 0.9 mm orifice size (see Table 3).

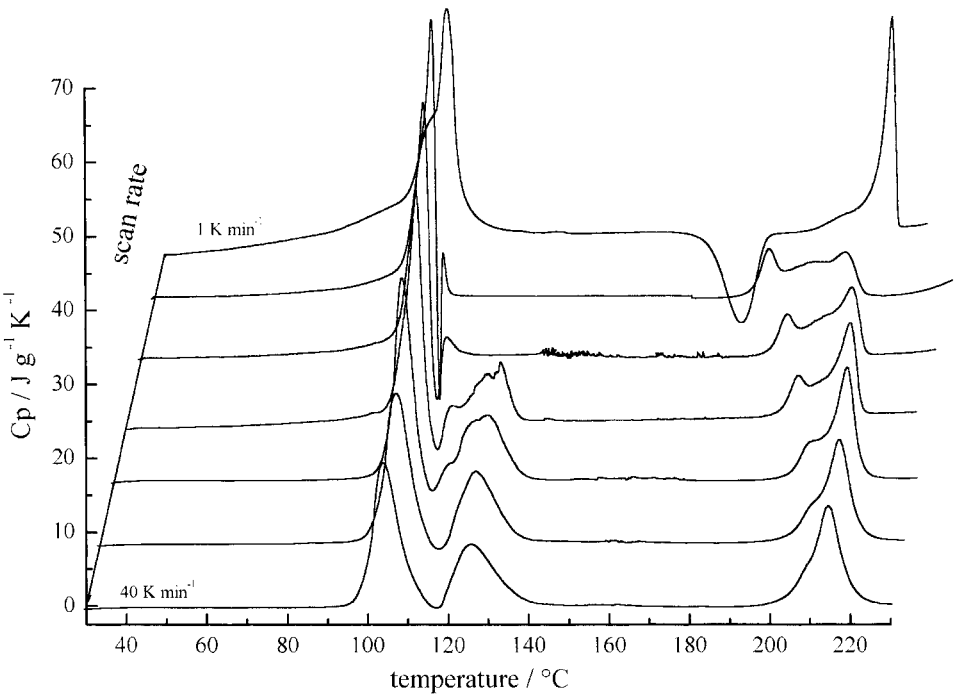

Fig. 6. DSC curves of TRE_h heated in cells with 0.5 mm orifice size at different scan rates (as in Fig. 4).

Table 4

Scan rate (K/min)	T_p (°C)	ΔH (kJ/mol)	T_p (°C)	ΔH (kJ/mol)	T_p (°C)	ΔH (kJ/mol)	T_p (°C)	ΔH (kJ/mol)
	$TRE_h \rightarrow TRE_{am}$				$TRE_{am} \rightarrow TRE_\beta$		$TRE_\beta \rightarrow TRE_L$	
1	100.3	95.2			173.2	−41.9	211.3	40.5
	$TRE_h \rightarrow TRE_{anh}$		$TRE_{anh} \rightarrow TRE_\gamma$		$TRE_\gamma \rightarrow TRE_\beta$		$TRE_\beta \rightarrow TRE_L$	
2	99.9	83.1	101.5	−0.2	102.6	3.5	183.7	50.5
5	101.1	71.1	104.1	−3.3	106.7	2.4	207.5	46.1
10	101.3	53.7	105.6	−2.3	121.7	34.2	210.4	47.5
20	102.1	57.7	109.5	−1.2	123.4	39.6	212.9	48.5
30	104.0	57.4	114.2	−1.0	123.6	36.0	213.9	46.6
40	103.7	59.8	117.3	∼0	125.7	36.2	214.7	47.0

Temperature and enthalpy changes for the transitions of trehalose at different scan rates.

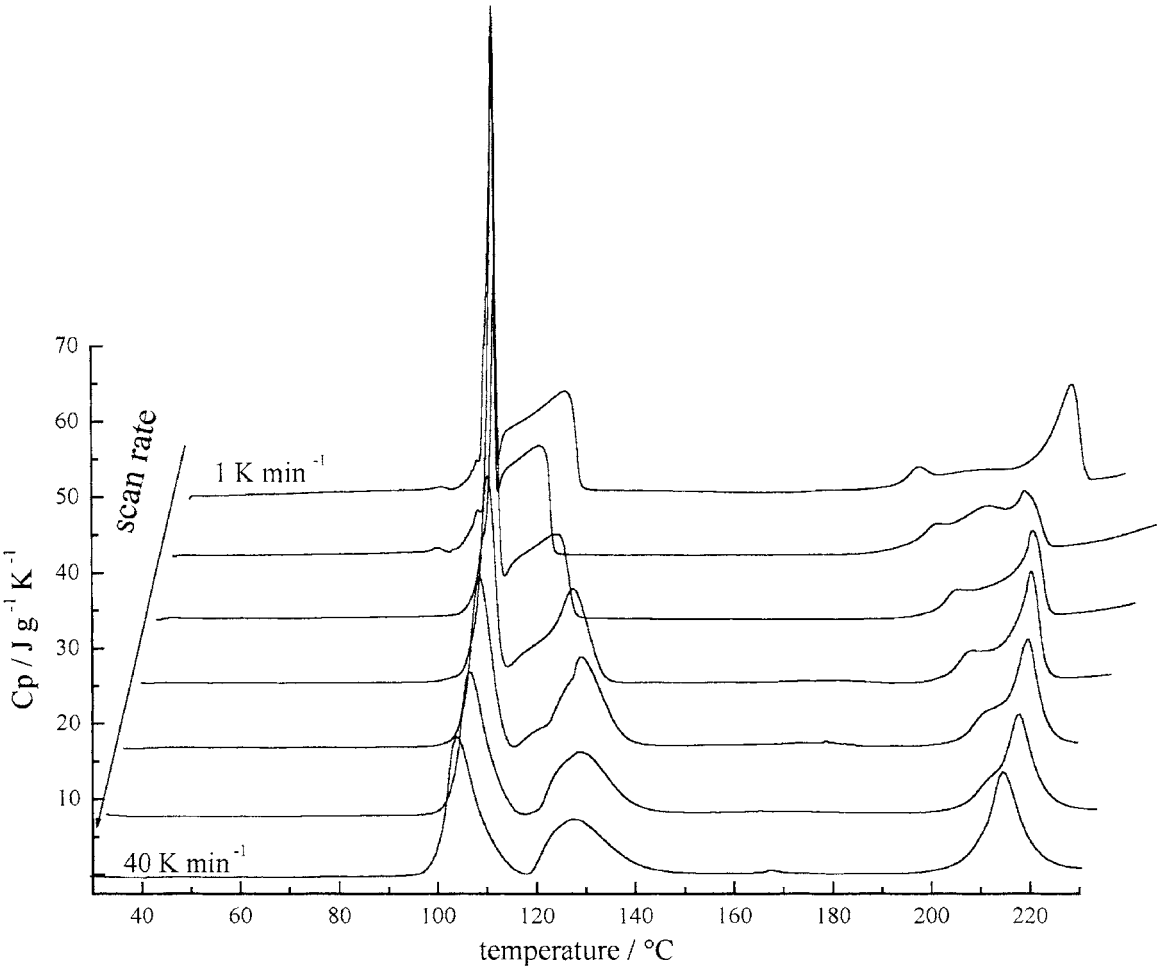

Fig. 7. DSC curves of TRE_h heated in cells with 0.1 mm orifice size at different scan rates (as in Fig. 4).

Table 5

Scan rate (K/min)	T_p (°C)	ΔH (kJ/mol)	T_p (°C)	ΔH (kJ/mol)	T_p (°C)	ΔH (kJ/mol)
	$TRE_h \rightarrow TRE_\beta$				$TRE_\beta \rightarrow TRE_L$	
1	93.2	97.5			209.0	41.5
2	95.0	94.9			202.9	45.8
5	98.4	89.3			207.5	42.7
10	100.3	90.7			210.5	44.1
	$TRE_h \rightarrow TRE_{am}$		$TRE_{am} \rightarrow TRE_\beta$		$TRE_\beta \rightarrow TRE_L$	
20	102.0	45.0	122.7	45.1	213.3	43.6
30	103.1	47.5	125.4	39.1	214.7	42.3
40	103.6	52.2	127.4	37.7	214.5	43.8

Temperature and enthalpy changes for the transitions of trehalose at different scan rates.

and more intense than the second one. Both peaks shift at higher temperature as the scanning rate is increased with a complete separation for a scan rate of 20 K/min. The high temperature peak is made up of several shoulders when the sample is heated slowly, but becomes symmetric as the scan rate increases.

The use of a sealed pan leads to results (Fig. 8 and Table 6) very different from those obtained with all the

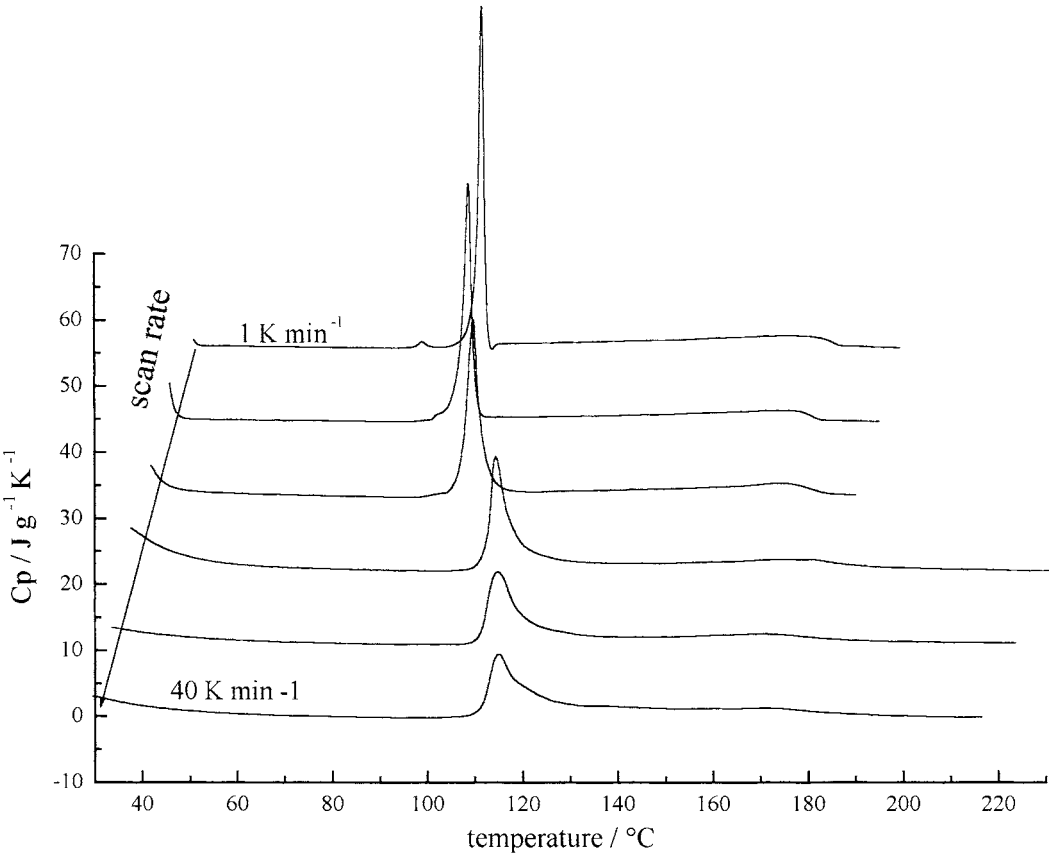

Fig. 8. DSC curves of TRE_h heated in sealed cells as a function of scan rate (1, 2, 5, 20, 30 and 40 K/min). Dehydration peak shape is scan rate dependent; no other polymorphic transitions are observed.

Table 6

Scan rate (K/min)	T_p (°C)	ΔH (kJ/mol)
	$TRE_h \rightarrow TRE_\beta$	
1	91.9	85.1
2	92.9	85.1
5	97.8	94.4
10	101.6	92.1
20	106.6	95.8
30	110.8	89.7
40	114.6	97.6

Temperature and enthalpy changes for the transitions of trehalose at different scan rates.

other types of pans and therefore a direct comparison of the data cannot be done. The reason of this difference relies upon the fact that, in this type of cells, melting of TRE_h occurs without effusion of water vapour from the cell (see solubility line of TRE_h in Fig. 1 of [4]). The area of the melting peak is small although very narrow at 1 K/min; increasing scan rates it becomes less intense and broader. In comparison with all the previous thermograms, the difference is the absence of any other significant thermal events above 100 °C, except a very broad endotherm at about 160 °C, due to partial equilibration (dehydration) of the liquid phase with molar fraction $X_{TRE} = 0.33$.

3.5. Rationale for dehydration process parameterisation

In order to rationalise the data here collected, further attention to the parameters governing the process is necessary. These parameters have been identified by using intuitive although compelling reasons for the comparison of the present process with the actual "in vivo" process of dehydration of living cells producing trehalose. A reasonable approach is to assume that, in addition to temperature, two more variables govern the process of water evaporation/effusion: one is the time scale of the process, which is measured by the inverse of the scanning rate; the other variable is the size of the "hypothetical" pores through which water effuses.

For each experiment, with a defined orifice size and a defined scan rate, the thermograms reported above (Figs. 4–8) present a number of thermal events which have already been assigned [10]. Transition temperatures for highly asymmetric peaks can only conventionally be taken. Therefore, peak temperatures have been arbitrarily chosen as "markers" for the phase transitions in the diagrams in Fig. 9A–C, showing transition temperatures as a function of the logarithm of the transformation time (taken as the inverse of scanning rate). In these diagrams low and high transformation times clearly produce different thermal paths; e.g. in Fig. 9B, the transitions TRE_γ–TRE_β and TRE_h–TRE_α–TRE_β, respectively are identified. An ill-defined zone in the middle range of $\log t$ is characterised by direct amorphisation of TRE_h. This information becomes very useful for processing TRE_h to obtain amorphous product without reaching high temperatures.

A cursory inspection on the results of the dehydration process at different scan rates and with different orifices (Fig. 9A–C) indicates that two events are constantly present and predominant. These phenomena are related to the processes of dehydration of TRE_h crystals and of melting of the TRE_β form. The first process appears to be influenced by scan rate since water leaving the crystalline structure is able to induce collapse or symmetry displacements in the original frame. A sort of thermal imprinting of the conditions used for this process is carved in the traces of the thermograms recorded above the temperature of dehydration. The last thermal transition is also influenced by the previous thermal history of the sample; however, the modifications seen in the transition peak of TRE_β to liquid fall in the common behaviour of the melting of crystalline phases which have been produced in different ways, i.e. by cold crystallisation or by solid–solid transition. In other words, the shape of the final melting peak is function of the perfection of the crystals, a property which is direct consequence of the mechanism of crystallisation.

For all the other processes located between the above two transitions (i.e. between 100 and 200 °C), the shape of the thermograms is more complex but still conceivable on the basis of the identification of the structural forms produced after each thermal event.

3.6. Dynamic transformation diagram

From the above results, it becomes clear that scan rates and orifice sizes affect transformation processes

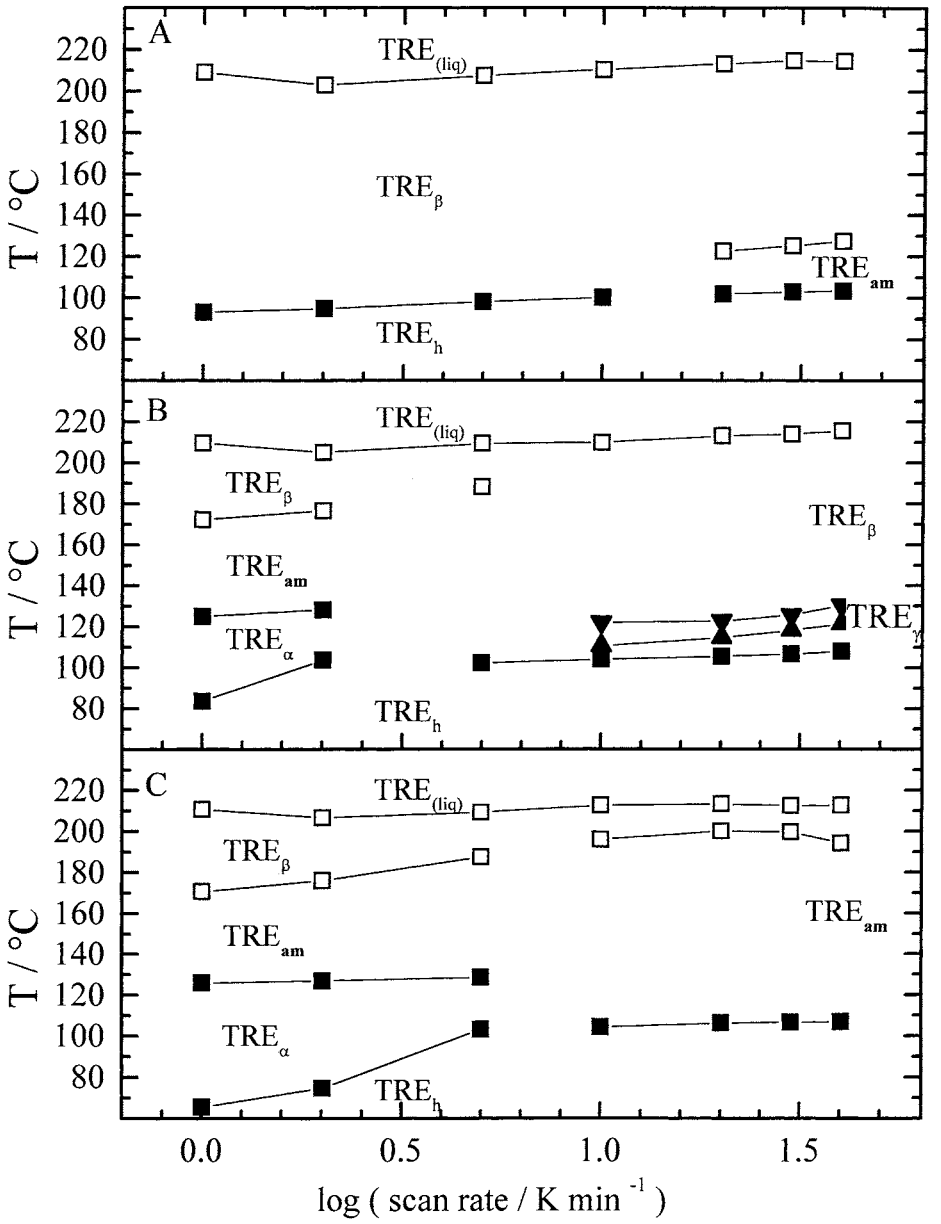

Fig. 9. Transition temperatures as a function of the logarithm of scan rate for cells with orifice size of (A) 0.1 mm; (B) 1.2 mm and (C) open cells. Open symbols are related to high temperature transitions involving TRE_{β}; open symbols are reated to dehydration of TRE_{h} and following transformations involving TRE_{α} and TRE_{γ}.

not only for the water escaping during the first thermal step (vapour effusion) but indirectly also by tuning water residence time upon heating scans (water plasticisation). Modulation of the two streaming variables (temperature scanning and water flowing) is the key action for the production of a given trehalose form. The rationale for the interpretation of these data is a diagram of transition temperature as a function of the time scale of trehalose transformations and the time-scale of water effusion. Although such a diagram is not

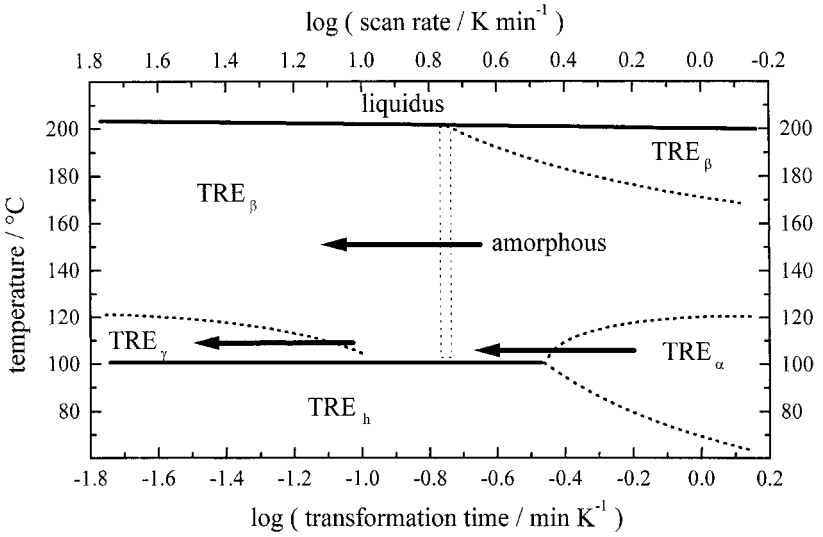

Fig. 10. Dynamic transformation diagram showing the dependence of transition temperatures and trehalose phases on the logarithm of transformation time (taken as the inverse of scan rate). Arrows show the variation of the coexistence lines with the changes in the orifice size.

at equilibrium, it is here referred to as ‘‘dynamic phase diagram’’ because it identifies a particular polymorph in a domain of temperature, scan rate and water effusion.

A schematic comprehensive plot is reported in Fig. 10, where the absissa is the inverse of the scan rate and, therefore, is the time for 1 K change. The dependence on the orifice size is traced by arrows showing the variation of the coexistence lines (dotted lines) with the changes in the orifice size. The position of these lines is directly related to the streaming variables. Although to the best of our knowledge, this kind of process/diagram has not been explored for other systems, the possibility that other hydrated carbohydrates or organic compounds undergo similar transformation processes is extremely interesting for many practical applications.

A further observation on the existence of an amorphous/glassy state is worth making at this stage of the discussion. According to the diagram of Fig. 10, amorphous state can be thermally produced under different ways: (a) by direct amorphisation of TRE_h; (b) by passing through the TRE_α form; (c) by cooling the liquid formed after melting TRE_β. Amorphisation temperature is always above the dehydration temperature at about 110 °C (case (a) or even at 130 °C (case (b). None of the experimental conditions reported could give the direct formation of a glass, unless the amorphous phase formed at high temperatures (110–130 °C) is then cooled back to ambient temperature. In our opinion this is an important matter that needs further experimental investigation to clarify whether the amorphous/glassy states have or not the role claimed in preservation.

On the other hand, TRE_α can be produced from TRE_h under gentle conditions of low scanning rates (large transformation times) and high orifice sizes (low humidity) at relatively low temperatures (possibly below 60 °C). The question on whether the formation of polymorph TRE_α and its reversible transformation to TRE_h is a relevant process in biopreservation has already been addressed in the literature [4].

4. Conclusions

The main result of this piece of work is a diagram which includes not only the ‘‘static’’ temperature/transformation coexistence lines but also their dependence on the time required for the transformations and the rate of vapour flowing out of the cell. This information is relevant for the best simulation of the natural process of dehydration ‘‘in vivo’’, which conceivably

occurs under slow heating and under controlled evaporation rate. However, no direct comparison or deduction is made here, at this stage of knowledge, without other appropriate data on solid constraints and thermal motions; mention is made only to give a further indication for the direction of future research in this field.

Acknowledgements

This work was supported by the University of Trieste and by CNR (Grant CT9800243). F.S. is grateful to INSTM (Florence) for supporting her Research Fellowship.

References

[1] A. Saleki-Gerhardt, J.G. Stowell, S.R. Byrn, G. Zografi, J. Pharm. Sci. 84 (1995) 318.
[2] E.A. Schmitt, D. Law, G.G.Z. Zhang, J. Pharm. Sci. 88 (1999) 291.
[3] K. Kajiwara, F. Franks, J. Chem. Soc., Faraday Trans. 93 (1997) 1779.
[4] F. Sussich, C. Skopec, J.W. Brady, A. Cesàro, Carbohydrate Res. 334 (2001) 165.
[5] J.H. Crowe, F.A. Hoekstra, L.M. Crowe, Ann. Rev. Physiol. 54 (1992) 579.
[6] M. Ferrando, W.E.L. Spiess, J. Food Eng. 49 (2001) 115.
[7] M.A. Singer, S. Lindquist, Trends Biotechnol. 16 (1998) 460.
[8] F. Sussich, R. Urbani, F. Princivalle, A. Cesàro, J. Am. Chem Soc. 31 (1998) 7893.
[9] F. Sussich, F. Princivalle, A. Cesàro, Carbohydrate Res. 322 (1999) 113.
[10] F. Sussich, A. Cesàro, J. Therm. Anal. Calorim. 62 (2000) 757.
[11] S.P. Ding, J. Fan, J.L. Green, Q. Lu, E. Sanchez, C.A. Angell, J. Therm. Anal. 47 (1996) 1391.
[12] J.F. Villart, A. De Gusseme, S. Hemon, G. Odou, F. Danede, M. Descamps, Solid State Commun. 119 (2001) 501.
[13] L. Yu, Adv. Drug Delivery Rev. 48 (2001) 27.
[14] K. Akao, Y. Okubo, N. Asakawa, Y. Inohue, M. Sakurai, Carbohydrate Res. 334 (2001) 233 (and previous work quoted therein).
[15] A.M. Gil, P.S. Belton, V. Felix, Spectrochim. Acta A52 (1996) 1649.
[16] G. Batta, K.E. Kover, Carbohydrate Res. 320 (1999) 267.
[17] A.K. Galwey, Thermochim. Acta 355 (2000) 181.
[18] L.S. Taylor, P. York, Int. J. Pharm. 167 (1998) 215.
[19] L.S. Taylor, A.C. Williams, P. York, Pharm. Res. 15 (1998) 1207.